

BACKGROUND CHARACTERIZATION AND STUDIES USING THE XIA
ULTRALO-1800
FOR DARK MATTER EXPERIMENTS

Approved by:

Dr. Jodi Cooley

BACKGROUND CHARACTERIZATION AND STUDIES USING THE XIA
ULTRALO-1800
FOR DARK MATTER EXPERIMENTS

A Senior Thesis Presented to the Undergraduate Faculty of the
Dedman College

Southern Methodist University

in

Partial Fulfillment of the Requirements

for the degree of

Bachelor of Science with Distinction

with a

Major in Physics

by

Mayisha Zeb Nakib

May 2015

ACKNOWLEDGMENTS

The author of this paper would like to thank Professor Jodi Cooley for taking her on as a student since her first week of college and allowing her to do research for all four years at Southern Methodist University. She would also like to thank Professor Stephen Sekula, Dr. Silvia Scorza, Dr. Rob Calkins, Hang Qui, Bedile Karabuga, along with Professor Cooley for teaching her so much with tremendous patience and encouraging her to grow as a physicist. She would like to thank Dr. Randall Scalise for help with several calculations. In addition, she would like to thank Dr. Rielage, Dr. Schnee, Dr. Guisepe, Kevin Ciexzowski, Tim Mulone, and Lacey Porter for their contributions. She would also like to thank Matthew Bruemmer for being an awesome co-minion.

This material is based upon work supported by the National Science Foundation under Grant Number (1151869), the SMU Hamilton Scholar program, and SMU Engaged Learning. Any opinions, findings, conclusions, or recommendations expressed in this material are those of the author(s) and do not necessarily reflect the views of the National Science Foundation.

Nakib , Mayisha Zeb

Background Characterization and Studies Using the XIA UltraLo-1800
for Dark Matter Experiments

Advisor: Professor Jodi Cooley

Bachelor of Science with Distinction degree conferred May 2015

Senior Thesis completed April 2015

Abstract:

Southern Methodist University houses one of the first five commercially available UltraLo 1800 production model alpha counters made by XIA LLC. The instrument has an electron drift chamber with a 707 cm² or 1800 cm² counting region which is determined by selecting the inner electrode size. The SMU team operating this device is part of the SuperCDMS screening working group, and uses the alpha counter to study the background rates from the decay of radon in materials used to construct the SuperCDMS experiment along with other rare event searches. We have also studied four acrylic samples obtained from the MiniCLEAN direct dark matter search with the XIA instrument demonstrating its utility in low background experiments by investigating the plate-out of ²¹⁰Pb and comparing the effectiveness of cleaning procedures in removing ²²²Rn progenies from the samples. We present results for two preliminary studies using a ²²⁰Rn source to expose copper samples. The first study compares ²²⁰Rn plate-out while samples are housed in an insulating glass jar verses a stainless steel pressure cooker. The second study compares radon mitigation using a 3 SCFH and 6 SCFH boil-off nitrogen purge rate inside a modified pressure cooker with a control experiment with no air flow.

TABLE OF CONTENTS

LIST OF FIGURES	vii
LIST OF TABLES	ix
CHAPTER	
1. INTRODUCTION	1
1.0.1. The ^{222}Rn Decay Chain	3
1.1. Equations Describing Radioactive Decay	5
1.1.1. Secular Equilibrium	6
2. THE INSTRUMENT: XIA ULTRALO-1800	7
2.1. A Sensitive Ionization Counter	7
3. TRAY EFFICIENCY WITH THORIUM SOURCE ..	11
4. EVALUATING CLEANING METHODS ON ACRYLIC SAMPLES	15
4.1. Counting and Cleaning of Acrylic Samples	15
4.2. Ingrowth Calculations	16
4.3. Results	19
5. COPPER IN A GLASS AND STAINLESS STEEL VESSEL	21
5.1. Alternative Source: Thorium-232 Decay Chain	22
5.2. Experiment Details.....	23
5.3. Results	25
6. REDUCTION OF RADON PLATE-OUT ON COPPER UNDER NITROGEN PURGE	31

6.1. Experimental Setup	31
6.2. Results	34
7. Study of Radon History in SuperCDMS at Soudan ...	37
8. Conclusion	42
APPENDIX	
A. Radon Monitoring in LUMINA Lab.....	44
B. Appendix: XIA Efficiency Correction	46
REFERENCES	47

LIST OF FIGURES

Figure	Page
1.1 Peruna the XIA Machine.....	2
1.2 Uranium Decay Chain.....	3
1.3 Detector Charge Collection, Ionization vs Recoil Energy, and Ionization Ratios for SuperCDMS.....	4
2.1 XIA Schematic.....	8
2.2 Pulse Shapes.....	10
3.1 Thorium Source Tray Positions.....	12
3.2 Efficiency by Position.....	14
4.1 Acrylic Sample from MiniCLEAN.....	16
5.1 Thorium Decay Chain.....	22
5.2 Camping Lantern Mantle.....	23
5.3 Glass and Stainless Steel Exposure Vessel.....	24
5.4 Maximum Activity.....	25
5.5 Copper from Pressure Cooker.....	26
5.6 Bismuth Decay.....	28
5.7 Polonium Decay.....	29
6.1 Copper Holders.....	32
6.2 Purge Experiment Set Up.....	33
6.3 Copper Placement.....	34
6.4 Purge Experiment Results.....	36

7.1	Background Detector Activity	40
7.2	Towers for SuperCDMS Soudan	40
A.1	Radon in Lab	45

LIST OF TABLES

Table		Page
3.1	^{230}Th Source Runs	13
4.1	Acrylic Sample Measurement Summary	16
4.2	Acrylic Sample Ingrowth Summary	19
4.3	Acrylic Sample Peak Activity Prediction.....	20
5.1	Copper Exposed in Stainless Steel Pressure Cooker	27
5.2	Copper Exposed in Glass Jar	27
6.1	Emissivities at the 40th Hour of Measurement for Purge Experiments ..	35
7.1	Radon Exposure at SuperCDMS Facilities	38

This thesis is dedicated to my mother, Evan Zeb Nakib, for all her support and love.

Chapter 1

INTRODUCTION

Radon-222 (^{222}Rn) is the primary background of concern for direct dark matter searches and neutrinoless double-beta decay experiments. The noble gas is present in the air and accumulates in basements and underground facilities since it is heavier than nitrogen air. The decay daughter products of ^{222}Rn are charged and can easily stick to a detector component surface and remain fixed. Once on the surface of a detector, gamma, beta, and alpha particles along with recoiling nuclei from radioactive chains can mimic the desired signals in low radioactivity experiments. One of radon's decay products is lead-210 (^{210}Pb) which has a long half life of 22.3 years. It is infeasible to wait for the ^{210}Pb contamination to decay away in the lifetime of an experiment. Thus, the understanding of radon plate-out, or how radon progenies stick to surfaces is of crucial importance as is the reduction of radon exposure in the production, shipment, and storage of detector components.

The Laboratory for Ultra-pure Material, Isotope and Neutron Assessment (LUMINA) at Southern Methodist University houses one of the first five production model XIA UltraLo-1800 alpha particle counters inside a class 100 cleanroom (Fig. 1.1). The instrument is used to characterize backgrounds in various materials used in the construction of dark matter experiments, to study plate-out onto surfaces and to evaluate cleaning procedures.

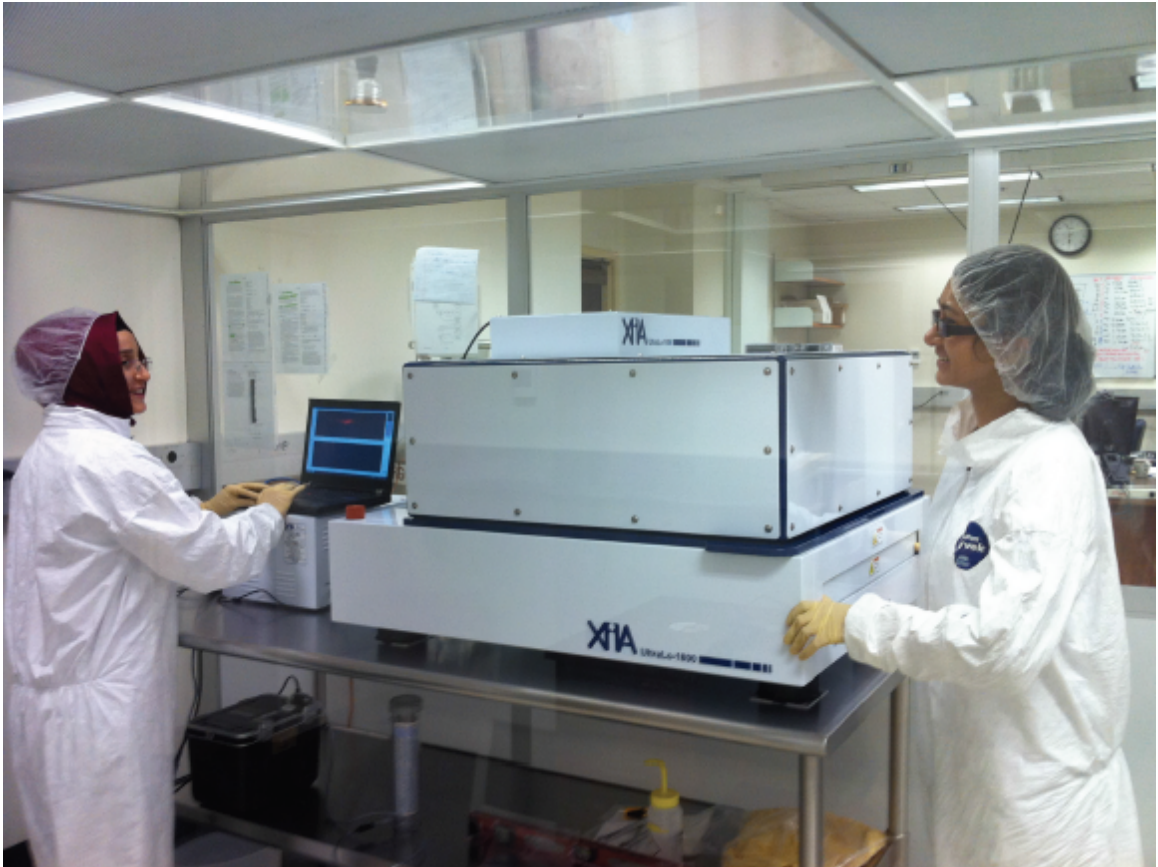


Figure 1.1. This is Peruna, the XIA UltraLo-1800 at Southern Methodist University

1.0.1. The ^{222}Rn Decay Chain

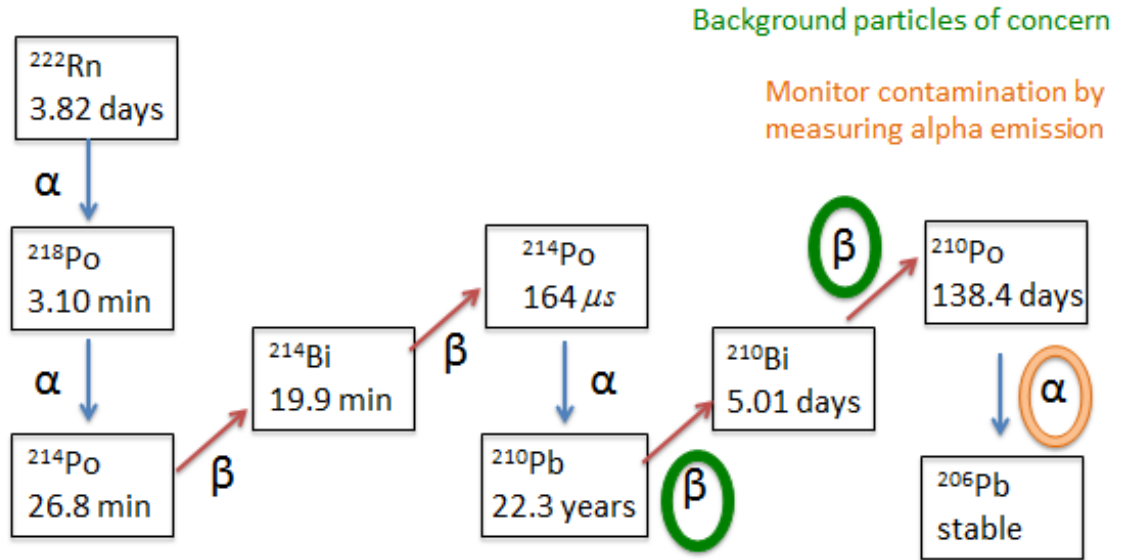


Figure 1.2. This diagram of the uranium-238 (^{238}U) decay chain is truncated at ^{222}Rn , the primary source of background for dark matter experiments.

As ^{222}Rn decays into charged daughter products, the daughter atoms can remain fixed onto detector surfaces and mimic desired signals. In solid state detectors like in the Super Cryogenic Dark Matter Search (SuperCDMS), the beta particles (emitted electrons), gamma particles (emitted photons), and the recoiling ^{206}Pb nucleus can mimic the nuclear recoil signature from a theoretically predicted dark matter particle called the Weakly Interacting Massive Particle or WIMP. This is illustrated in Figure 1.3. These background particles follow from the decay sequence after the long lived ^{210}Pb . The nuclear recoil from ^{206}Pb has a ratio of ionization yield and recoil energy that is close to the WIMP search nuclear recoil band as shown in Fig 1.3. Thus, ^{222}Rn is a significant contribution to backgrounds in the SuperCDMS experiment and other

dark matter or rare event searches. The XIA UltraLo can measure contamination from the ^{222}Rn by detecting a 5.3 MeV alpha particle emitted from ^{210}Po .

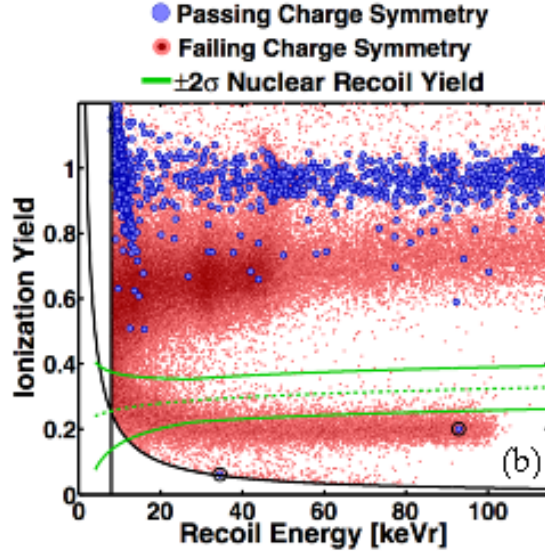


Figure 1.3. Ionization yield vs recoil energy after a ^{210}Pb calibration source is placed facing side 1. The blue dots are charge symmetric on both sides of the detector and came from inside the detector's germanium crystal. The red dots are not charge symmetric and arise from surface events. These red dots include betas, gammas, and the ^{206}Pb nuclei recoils. The green lines enclose the nuclear recoil band that represents the desired signal region. The upper red band of events are from betas and gammas. Recoiling of the ^{206}Pb nuclei form the red dots below the green band. As you can see, these events are very close to the desired signal range.[6]

1.1. Equations Describing Radioactive Decay

In a decay chain, the parent atom decays into a daughter atom and the activity from the parent atom, A_1 , is simply the time derivative of the number of parent nuclei N_1 ¹.

$$A_1 = -\frac{dN_1}{dt} = \lambda_1 N_1 = A_1^0 e^{-\lambda_1 t} \quad (1.1)$$

The eigenvalue λ_1 is the decay constant for the parent nuclei and is equal to natural log of 2 divided by the half-life. A_1^0 is the initial activity from the parent atoms. And the number of parent nuclei is:

$$N_1 = N_1^0 e^{-\lambda_1 t} \quad (1.2)$$

Here, N_1^0 represents the initial number of parent nuclei. The activity of the daughter nuclei is then determined by two components. The daughter atoms decay exponentially just as the parent atoms decay but with a different decay constant λ_2 that corresponds to the daughter atom's half life. But, the supply of daughters increases as the parent nuclei decays:

$$\frac{dN_2}{dt} = -\lambda_2 N_2 + \lambda_1 N_1 \quad (1.3)$$

The solution to the above differential equation is the number of daughter nuclei:

¹All equations in this chapter follow the style of [5]

$$N_2 = \frac{\lambda_1}{\lambda_2 - \lambda_1} N_1^0 (e^{-\lambda_1 t} - e^{-\lambda_2 t}) + N_2^0 e^{-\lambda_2 t} \quad (1.4)$$

N_2^0 represents the initial number of daughter nuclei at $t = 0$ which is usually directly after a sample's exposure to a radioactive source. And the daughter activity is:

$$A_2 = \lambda_2 N_2 = \frac{\lambda_2}{\lambda_2 - \lambda_1} A_1^0 (e^{-\lambda_1 t} - e^{-\lambda_2 t}) \quad (1.5)$$

1.1.1. Secular Equilibrium

Secular equilibrium occurs when the parent nuclei's half life is significantly longer than the daughter nuclei's half life. In cases of secular equilibrium $\frac{\lambda_2}{\lambda_2 - \lambda_1}$ term simplifies to one giving:

$$A_2 = A_1^0 (e^{-\lambda_1 t} - e^{-\lambda_2 t}) \quad (1.6)$$

Since the parent half life can be thought of as infinitely longer than the daughter half life, as time goes on, the number of parent nuclei stays about the same. The number of daughter nuclei however increases. As a result the total activity over time tends to increase after initial exposure. As time t approaches ∞ , the activity of both the parent nuclei and daughter nuclei are equivalent [5]. After an activity peak, both activities begin to decrease.

THE INSTRUMENT: XIA ULTRALO-1800

2.1. A Sensitive Ionization Counter

The XIA UltraLo-1800 alpha counter is a specialized ionization counter comprising of an active volume filled with argon, a lower grounded electrode that is a conductive tray holding the sample, and an upper pair of positively charged electrodes [8]. Of these two electrodes, the anode sits above the sample, while the one-inch guard electrode surrounds and encloses the anode. Both electrodes are connected to charge-integrating preamplifier whose output signals are digitized and then processed by a digital pulse shape analyzer (Fig. 2.1). When alpha particles are emitted from the sample on the tray, the alpha particles ionize the argon gas in the chamber. The released electrons drift up the chamber due to the potential difference and induce a current in the electronics above.

The XIA counter has a drift chamber that is 15 inches tall and 21 inches on both sides. There are two possible configurations for the counting region defined by an adjustable inner electrode size. The largest is an 1800 cm² square area and the other is a 707 cm² circular area. The instrument is purged with boil-off gas from a liquid argon dewar. After opening the tray, the counter is purged with 20 L/m for at least forty-five minutes before taking data. All pre-measurement purge times prior to August 26, 2014 were forty-five minutes long. However, this minimum purge time was not enough to remove electronegative oxygen and water vapor from the chamber after opening the tray. The oxygen can trap some electrons preventing them from

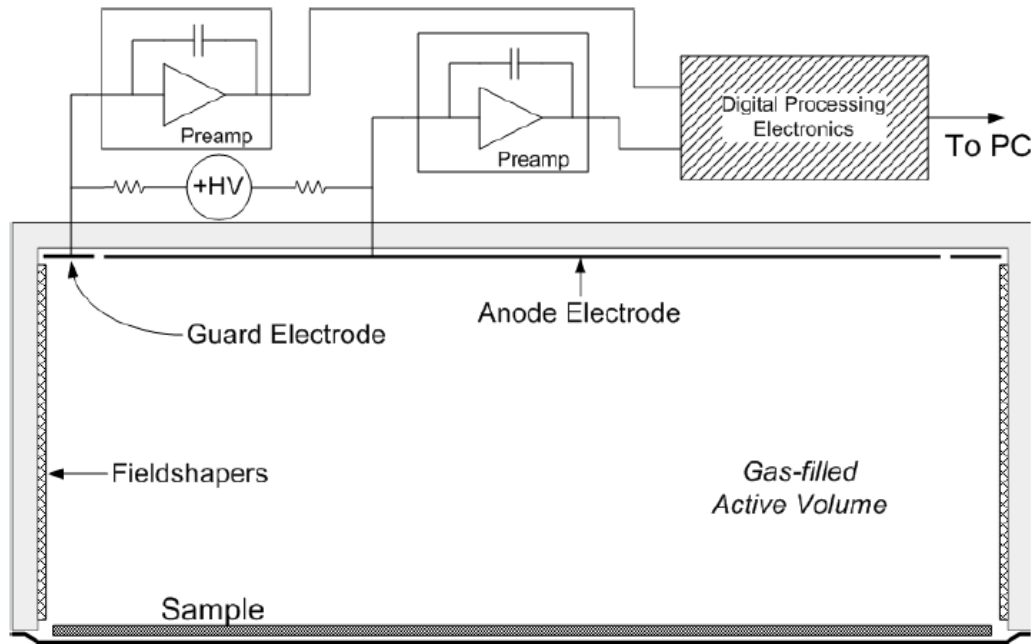


Figure 2.1. XIA alpha counter schematic from the User's Manual [4]

being detected. Samples counted after August 2014 use a one hour pre-measurement purge if the tray has been opened. In cases where the sample out-gases oxygen in the chamber or the lab air is particularly humid longer purge times may be used. During normal operation and during measurements, the counter is purged with 4 L/m of argon gas [4].

Unlike proportional counters, the XIA counter has the ability to distinguish alpha events emitted from the tray from alpha events emitted from the ceiling or sidewalls of the drift chamber by using pulse-shape discrimination, rise time selection, and guard anode activity [1]. Alpha events detected from the sample tray have energy greater than 2 MeV, little guard ring activity, and a pulse rise time between between 40-80 μ s.

Alpha events from the anode (ceiling) and the sample (cathode) are discriminated based on rise time and signal amplitude provided that the separation between the cathode and the anode is significantly greater than the range of alpha particles in argon (~ 5 cm at standard temperature and pressure for a 4.5 MeV alpha). The sidewall events have a higher guard ring activity than anode activity. These event types are illustrated in Fig 2.2. If an alpha event from the sample tray and part of its ionization track fall under the guard electrode, it cannot be distinguished from a sidewall event. To account for this, the XIA company provides an efficiency correction based on analytical computations, Monte Carlo simulations, and measurements with a calibrated source. These corrections are included in the appendix [4]. However, since this efficiency correction assumes the sample covers the entire 707 cm² or 1800 cm² area and all of the samples counted in this thesis are smaller than the entire tray area, this efficiency correction is not used in this thesis. The XIA counter also distinguishes cosmogenic events which have a rounded pulse shape, mid-air events from the gas in the counter which have a shorter rise time, and noise events which do not fit into any other classification [4].

The instrument went under standard studies comparing its performances to the other XIA alpha counters in December 2012. Three different samples were counted in all of the existing XIA alpha counters at the time including a sixth counter owned by XIA [2]. It has been confirmed that the SMU alpha counter results agree within 1σ with the results of the other existing alpha counters for two of the samples, an aluminum alloy wafer and a titanium wafer. For the third sample, a silicon wafer, the results from SMU agreed within 1σ with 3 other alpha counters at other locations while two of the alpha counters had higher results. The differences between the alpha counters can be explained from counting statistics and differences in the amount of overburden at each facility. This suggests there is some component of background

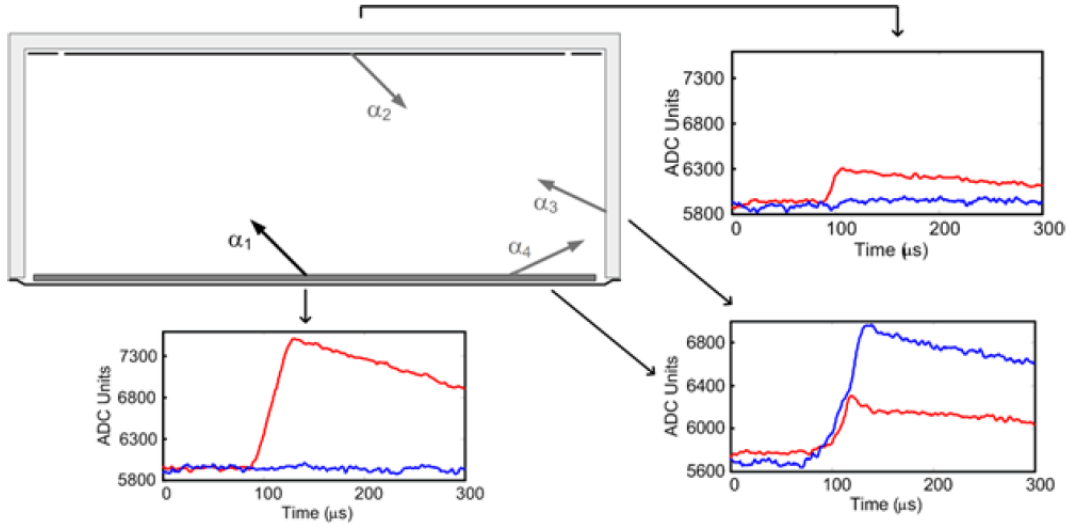


Figure 2.2. Alphas originating from various locations in the counter and their corresponding anode (red) and guard (blue) pulse shapes. 1 shows a sample alpha, 2 shows a ceiling emission, and 3 shows a sidewall emission, and 4 shows a sample alpha that travels under the guard. Image from the User’s Manual [4].

from cosmogenics that are not rejected due to rounded pulse shape. SMU’s alpha counter operates in a cleanroom in a basement lab of concrete construction with an estimated overburden of 2195 g/cm^2 .

Measurements of the background level resulting from the empty tray are taken regularly in between various samples and over weekends. In order to keep our sensitivity as low as possible we are currently operating with the stainless steel tray covered with a layer of conductive Teflon. This has reduced and stabilized the counter background to $0.0011 \pm 0.0003 \text{ alpha}/(\text{h cm}^2)$. Maintenance of the tray involves wiping the stainless steel tray and the Teflon with a Radiacwash towelette, rinse with a cleanwipe squirted with deionized water, and then wipe with isopropyl alcohol.

Chapter 3

TRAY EFFICIENCY WITH THORIUM SOURCE

The XIA LLC company provides an efficiency correction due to mischaracterized "sidewall" pulses that are actually from the sample as mentioned in Chapter 2. However, this efficiency correction is specific to samples that cover the entire tray area. Since the majority of samples we count are smaller than the wafer sized configuration, it was necessary to study the collection efficiency in various parts of the tray with a point-like source. A study with a calibrated ^{230}Th source with a known activity was performed in order to study the XIA alpha counter's collection efficiency. This was necessary to determine whether or not the collection efficiency is symmetric about the polar angle as we expect from the machine's geometry. We also investigated how the collection efficiency changed as the source was moved from the center of the tray to the edge. We acquired sets of ninety-minute measurements with the ^{230}Th source placed in different positions on the empty tray and analyzed the results by comparing the ^{230}Th source emissivity to the experimentally recorded emissivity in the region of interest around 4.8 MeV. Seven positions, called W1 through W7 (Fig. 3.1), were studied and rulers were used to guide placement of the samples onto the tray. Empty tray measurements were taken overnight in order to monitor the environmental background. Two sets of data were taken for the positions and compared to the source's emissivity of $1022 \pm 4\%$ alphas (h / cm^2) for a 2π solid angle given by the manufacturer. (The one-inch diameter source has a 4π activity of $2.977 \pm 4.4\%$ Bq). The emissivity and efficiencies are reported in Table 3.1 for the 2-10 MeV range and the region of interest between 4 and 6 MeV.

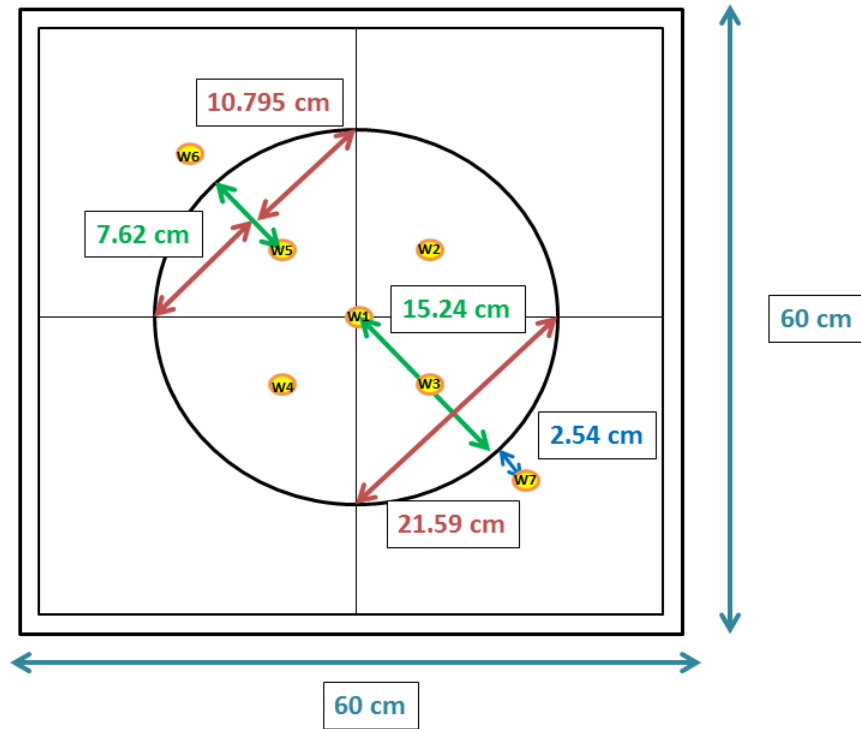


Figure 3.1. Seven tray positions studied using a calibrated ^{230}Th source with the smaller wafer electrode size. Position W1 is in the center. W3 through W5 are located half way between the center and outer circumference of the smaller 707 cm^2 counting region. Note that position W1 and W7 are outside of the wafer counting region. All measurements to the thorium source are to the center of the thorium source. The radius of the thorium source is half an inch so to measure to the edge of the source is to subtract half an inch (1.27 cm) from these numbers.

Run Name	2-10 MeV Range		4-6 MeV Range	
	Emissivity ($\alpha/(\text{h cm}^2)$)	2π Efficiency (%)	Emissivity ($\alpha/(\text{h cm}^2)$)	2π Efficiency (%)
W1	865_{-8}^{+8}	84_{-3}^{+3}	758_{-7}^{+7}	74_{-3}^{+3}
W2	834_{-8}^{+8}	81_{-3}^{+3}	713_{-7}^{+7}	69_{-3}^{+3}
W3	814_{-8}^{+8}	79_{-3}^{+3}	681_{-7}^{+7}	66_{-3}^{+3}
W4	841_{-8}^{+8}	82_{-3}^{+3}	714_{-7}^{+7}	69_{-3}^{+3}
W5	787_{-8}^{+8}	77_{-3}^{+3}	661_{-7}^{+7}	64_{-3}^{+3}
W6	$0.5_{-0.2}^{+0.3}$	$0.05_{-0.02}^{+0.03}$	$0.13_{-0.08}^{+0.21}$	$0.01_{-0.01}^{+0.02}$
W7	$1.1_{-0.3}^{+0.4}$	$0.11_{-0.03}^{+0.03}$	$0.13_{-0.08}^{+0.21}$	$0.01_{-0.01}^{+0.02}$
Empty Tray*	$0.37_{-0.07}^{+0.09}$	$0.04_{-0.01}^{+0.01}$	$0.09_{-0.03}^{+0.05}$	$0.009_{-0.003}^{+0.005}$

Table 3.1. Emissivities and Efficiencies for various ^{230}Th source positions on the wafer sized tray configuration show the collection efficiency is symmetric about the polar angle and decreases away from the center of the tray. Here the empty tray is treated as if it is only 1 inch in diameter to compare it to the thorium source emissivity. In actuality, the average of the three empty tray measurements taken is 0.0018 ± 0.0010 $\alpha/(\text{cm}^2 \text{ h})$ using the 707 cm^2 wafer sized tray configuration.

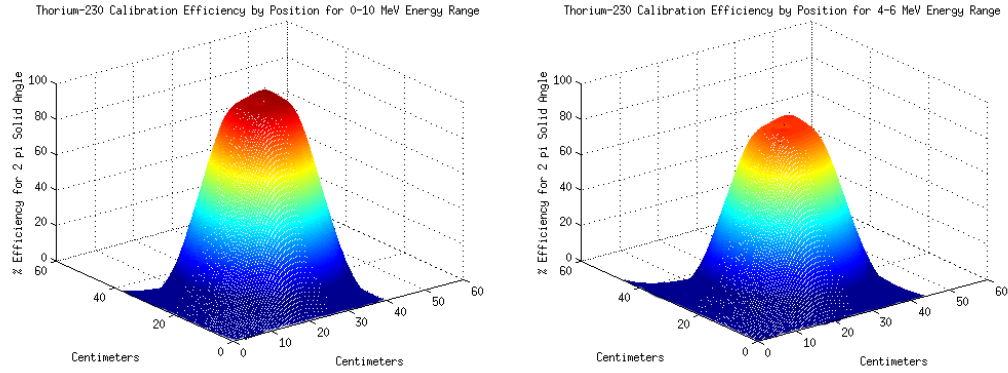


Figure 3.2. Left panel: Thorium-230 calibration efficiency by position for the 2 -10 MeV energy range compared to the calibrated source emissivity of $1020 \pm 40 \alpha/(\text{h cm}^2)$. Right panel: The same comparison of efficiency by position but for the 4-6 MeV region of interest.

The tray efficiency is symmetric around the polar angle within total statistical and systematic uncertainty, as expected. The measurements for W6 and W7 are consistent with the empty tray. In addition, the charge collection efficiency decreases as the thorium source is placed further from the center of the tray. The average efficiency of the charge collection is shown in Fig. 3.2. In the future, this study will be repeated using more measurements at different radii to improve the accuracy of the efficiency map. This correction map will be applied to small samples that do not cover the entire wafer or full sized tray area. Since more measurements need to be taken to create an accurate efficiency map, none of the studies in this report take this correction into account.

EVALUATING CLEANING METHODS ON ACRYLIC SAMPLES

4.1. Counting and Cleaning of Acrylic Samples

Four acrylic samples obtained from the MiniCLEAN direct dark matter search have been counted with the XIA instrument to investigate the plate-out of ^{210}Pb onto acrylic and to compare the effectiveness in removing ^{222}Rn progenies from the samples with different cleaning procedures. The six-by-six-inch square and one eighth inch thick acrylic samples (Fig. 4.1) were exposed to a ^{222}Rn source for 15 days, from September 1st to September 16th, 2011 by the MiniCLEAN collaboration. The samples were labeled AC01, AC02, AC03, and AC04. After exposure, the samples were sent to SMU to be counted with the XIA alpha counter. After counting, they were sent to MiniCLEAN to be cleaned. AC01 was cleaned by plasma etching by an IntIVac; AC02 and AC03 both had the top most 1 mm layer of acrylic shaved off, and AC04 served as the control sample with no cleaning procedure applied. Then, the samples were sent back to SMU to be counted again and monitored over time. The emissivities of the samples are reported in Table 4.1.

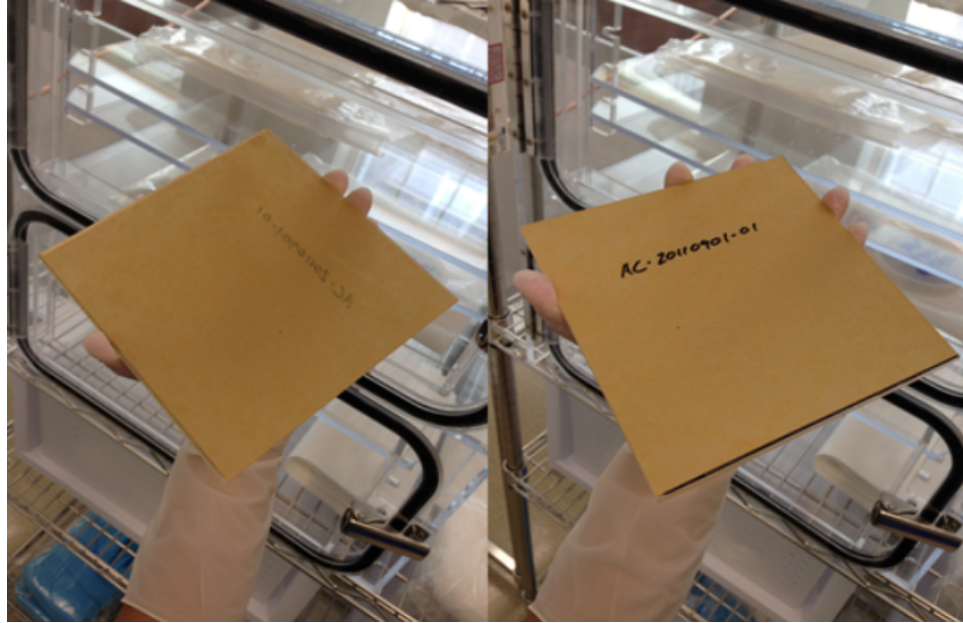


Figure 4.1. Left: Acrylic side that is counted in the UltraLo-1800. Right: Bottom paper film, not counted in the UltraLo-1800

SAMPLE	2-10 MeV		4-6 MeV (ROI)	
	Before Cleaning (alphas/(h cm ²))	After Cleaning (alphas/(h cm ²))	Before Cleaning (alphas/(h cm ²))	After Cleaning (alphas/(h cm ²))
AC01	$0.67^{+0.01}_{-0.01}$	$0.400^{+0.009}_{-0.009}$	$0.517^{+0.010}_{-0.010}$	$0.271^{+0.007}_{-0.007}$
AC02	$0.72^{+0.01}_{-0.01}$	$0.054^{+0.003}_{-0.003}$	$0.61^{+0.01}_{-0.01}$	$0.036^{+0.003}_{-0.003}$
AC03	$1.25^{+0.02}_{-0.02}$	$0.063^{+0.003}_{-0.003}$	$0.89^{+0.01}_{-0.01}$	$0.044^{+0.003}_{-0.003}$
AC04	$0.82^{+0.01}_{-0.01}$	$0.87^{+0.01}_{-0.01}$	$0.72^{+0.01}_{-0.01}$	$0.59^{+0.01}_{-0.01}$

Table 4.1. A summary of measurements for all samples counted in the XIA UltraLo-1800 before and after cleaning

4.2. Ingrowth Calculations

Ingrowth calculations have been performed for the time between the samples exposure and sample counting at SMU. Since earlier decay products have relatively short half-lives, we assumed that all of the radon daughter products that plated-out onto the acrylic samples were from ^{210}Pb for these calculations. We also assume that there were zero ^{210}Po before the end of the sample exposure. The alpha particles detected by the XIA counter must be from ^{210}Po since it is the only isotope after ^{210}Pb that emits alphas. The half life of the parent ^{210}Pb is 22.20 years while the half life of the daughter ^{210}Po is 138.37 days. Since the parent half life is significantly greater than the polonium half life, secular equilibrium conditions apply [5]. We can find the number of polonium atoms on our sample by dividing emissivity measured with the XIA counter by the daughter's decay constant. The decay constant for the lead parent and polonium daughter are as follows:

$$\lambda_1 = \frac{\log(2)}{(22.20)(365.25)} \quad (4.1)$$

$$\lambda_2 = \frac{\log(2)}{138.37} \quad (4.2)$$

We assumed all the samples were cleaned on May 24, 2012 and assumed that the cleaning method used is nondiscriminatory resulting in an equal number of polonium and lead atoms removed after cleaning. From there, we can use equations for ingrowth to find the increase of polonium over time and deduce the fraction of atoms removed by cleaning methods. The percent ingrowth reported here is the ratio of polonium and lead activity and is calculated as follows:

$$\text{ingrowth} = \frac{A_2(t)}{N_1^0 \lambda_1} = \frac{A_1^0(e^{-\lambda_1 t} - e^{-\lambda_2 t})}{N_1^0 \lambda_1} \quad (4.3)$$

Since we assume there are no initial polonium atoms present directly after exposure $N_2^0 = 0$. The emissivity in days is the measured activity A_{XIA} after t days from exposure. Before cleaning, 1.6 and A_{XIA} are the same. When the samples are cleaned, a certain percentage of both parent and daughter nuclei are removed. The second round of counting in the XIA gives us the remaining activity. To access the efficiency of the cleaning procedure, Eq. 1.6 must be used to give the expected activity after t days since exposure if the samples were never cleaned. After cleaning, the ratio of atoms remaining is the same as the ratio of measured activity verses predicted activity without cleaning:

$$\text{Atoms remaining} = \frac{A_{XIA}}{A_2(t)} \quad (4.4)$$

Using the formula below to predict the growth of polonium daughter products where N represents the number of atoms per cm^2 , a 1 indicates the parent ^{210}Pb , a 2 indicates the daughter ^{210}Po , and a subscript 0 indicates the initial number of atoms, we can predict the peak of emissivity in days after the cleaning procedure and predict the emissivity by setting the derivative equal to 0 and solving for t :

$$N_2 = \frac{\lambda_1}{\lambda_2 - \lambda_1} N_1^0 (e^{-\lambda_1 t} - e^{-\lambda_2 t}) + N_2^0 e^{-\lambda_2 t} \quad (4.5)$$

The predicted emissivity is simply $N_2(t)\lambda_2$ with λ_2 expressed in h^{-1} .

4.3. Results

The resulting ingrowth and removed contamination is reported in the table 4.2:

Sample	Exposure Ends	1 st Count	Ingrowth	Date Cleaned	Ingrowth	2 nd Count	Removed Contamination
AC01	16-Sept-11	7-Feb-12	51.0%	24-May-12	70.6%	6-Jul-12	63 ⁺² ₋₂ %
AC02	16-Sept-11	24-Feb-12	54.9%	24-May-12	70.6%	9-Jul-12	96 ⁺⁴ ₋₈ %
AC03	16-Sept-11	22-Feb-12	54.5%	24-May-12	70.6%	15-Aug-12	96 ⁺⁴ ₋₇ %
AC04	16-Sept-11	29-Feb-12	56.0%	24-May-12	70.6%	6-Aug-12	41.9 ^{+0.9} _{-0.9} %

Table 4.2. We calculate the percent ingrowth between the date the exposure ended and the date the sample is counted at SMU. We take into account the ingrowth at the time of the second count to calculate the expected activity if the sample had not been cleaned prior to the second measurement. This way we can determine the amount of contamination removed by each cleaning method.

Interestingly, the control sample AC04 which was not cleaned had 41.9% of contamination removed. This is simply from shipping and handling and storing the sample under purge. This indicates that much of the contamination is loosely attached to the surface and can easily be dusted off. AC01 which was cleaned by plasma etching removes only about 20% more than the control. Shaving off 1 mm of material leaves only about 4% of the polonium and lead which is implanted deep into the sample. Over the next two years we will monitor the acrylic samples. We predict their peak activity to occur around 500 days after the source exposure ends as in Table 4.3.

Sample	Peak Emissivity ($\alpha/(\text{h cm}^2)$)	Days After Exposure
AC01	0.33	535
AC02	0.044	532
AC03	0.74	499
AC04	0.32	507

Table 4.3. Using equation 4.5, the predicted peak activity is calculated after around 500 days after sample exposure ends. These values will be compared to future measurements

Chapter 5

COPPER IN A GLASS AND STAINLESS STEEL VESSEL

In the Super Cryogenic Dark Matter Search (SuperCDMS), copper shielding surrounds the detector towers and copper forms the case for the germanium detectors. Thus, copper has a direct line of sight with the dark matter detectors themselves. Understanding radon plate-out onto copper is necessary to understanding background activity in the SuperCDMS experiment. We tested whether radon progeny adhere to surfaces differently when surrounded by an insulator or a conductor. In this study we use a glass and a stainless steel exposure vessel with a radioactive source to expose a 6 x 4 inch copper rectangle placed on an inverted plastic cup. This study also served as a feasibility test to see if the camping lantern mantles could produce a measurable signal in the XIA UltraLo-1800 and hence could be used as a source for future studies.

5.1. Alternative Source: Thorium-232 Decay Chain

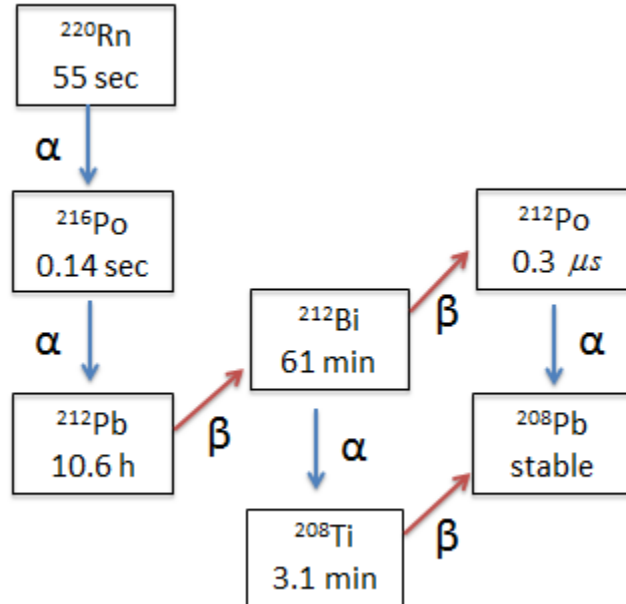


Figure 5.1. Thorium Decay Chain. Note the short half-lives in comparison to the uranium chain in 1.2

^{222}Rn is the isotope of interest to dark matter experiments because it has long lived progeny that cause the majority of background activity in dark matter experiments. However, our license to use a calibrated ^{222}Rn source was not approved in time for these studies. For this reason, we decided to conduct preliminary studies using pre-1990's camping lantern mantles (Fig.5.2) purchased from Old Coleman Parts that contain ^{232}Th as our radioactive source. (Fun trivia: The thorium supposedly made the fabric burn brighter. We have not bothered confirming if this is true). This alternative decay chain has short half-lives so, we do not need to calculate ingrowth to compare results. In addition, monitoring the decay of daughters to background

levels in the XIA counter happens in a matter of days. In contrast, it takes several years for the activity to reach the XIA counter's background levels when using the ^{222}Rn chain.



Figure 5.2. Camping Lantern Mantle from oldcolemanparts.com

5.2. Experiment Details

Each 6 x 4 inch copper rectangle had been exposed to 4 camping lantern mantles which are placed at the bottom of the exposure vessel. The glass jar was 30.5 cm tall and 22.9 cm in diameter. The stainless steel pressure cooker was 18.5 cm tall with a radius of 10.5 cm. The copper rectangle was placed on an inverted plastic cup that is 10.8 cm tall. The copper stored in the pressure cooker had been exposed from June 21, 2013 to October 17, 2013. The other copper had been stored in the glass jar from June 21, 2013 to November 14, 2013. The experiment set up is shown in Fig 5.3.



Figure 5.3. Exposure setup for studying insulating vs conducting housing.

In Fig 5.4., we see that the maximum activity is the production rate of the radioactive nuclei from the source. After three half lives, the maximum attainable activity had already been reached. This means the volumes inside the pressure cooker and inside the glass vessel had the same activity rate since the exposure times are a few months for both vessels. This is well over three times the 3.6 day half-life for radium from the thorium chain and all successive isotopes. This also means that the effects due to differences in exposure times can be neglected. In this study the exposure vessels have different volumes. To compare the insulator and conducting housing, we only consider the column height above the copper. This was simply the cylindrical volume above the inverted cup. For the glass jar, this was $8.04 \times 10^{-3} \text{ m}^3$. For the

pressure cooker, the column height volume was $2.67 \times 10^3 \text{ m}^3$. One critical assumption for this study was that the activity per camping lantern mantle is the same since they were manufactured with the same process. However, we do not know if this is actually true.

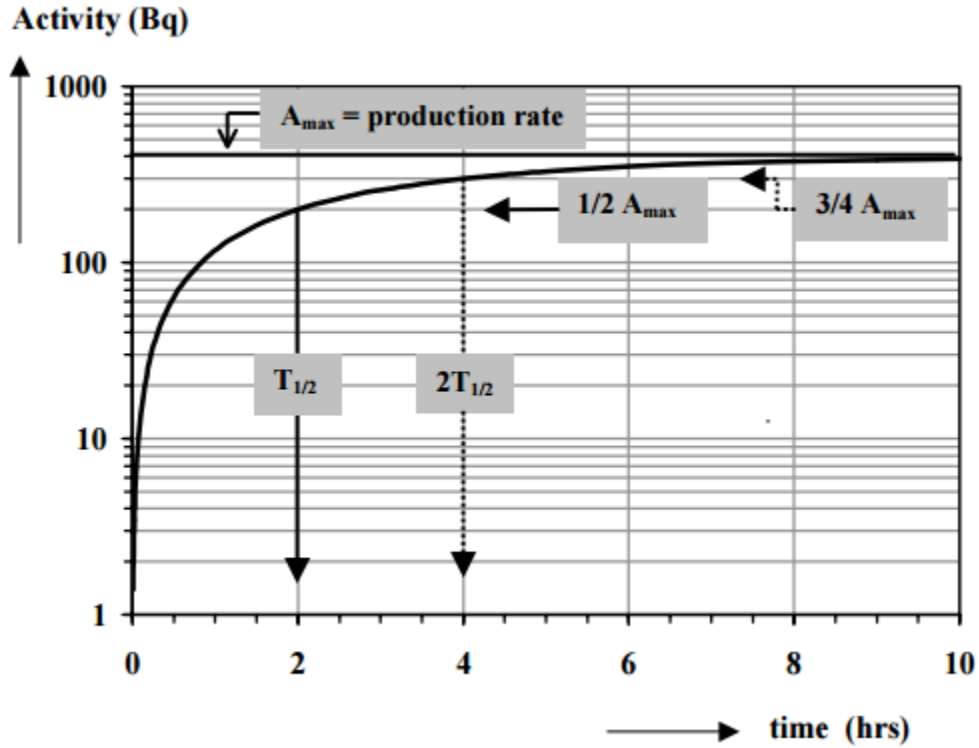


Figure 5.4. Reaching maximum activity for a half-life of two hours. Image from [5]

5.3. Results

The results for both exposure vessels show high activities. In fact, the first three days of post-exposure counting data in the XIA UltraLo-1800 were so high that the data acquisition laptop for the alpha counter ran out of RAM to store the events.

Using the camping lantern mantles as an exposure source for copper certainly gave measurable signals in the XIA UltraLo-1800. We immediately recognize two peaks at 6.2 and 8.9 MeV corresponding to ^{212}Bi and ^{212}Po respectively illustrated in Fig 5.5

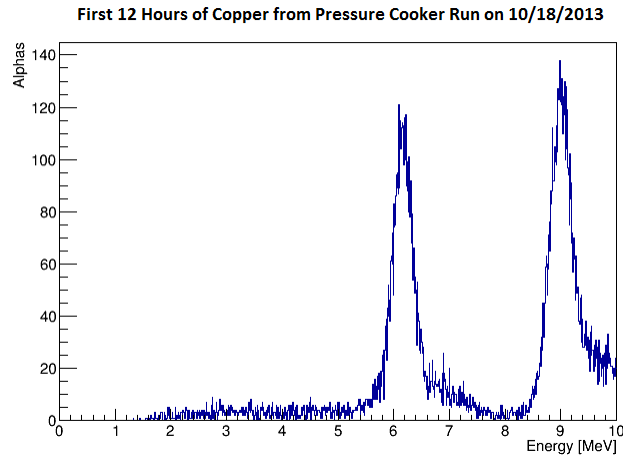


Figure 5.5. Counts per energy bin from the first 12 hours of the second measurement for copper stored in the pressure cooker. There are two strong peaks corresponding to alphas characteristic of ^{212}Bi and ^{212}Po . Both of these decay away in about 8 days.

The emissivities for the first four measurements with each piece of copper are shown in Table 5.1 and 5.2

Days After Exposure	Run Duration (h)	Total Emissivity ($\alpha/(\text{h cm}^2)$)	5-7 MeV Range ($\alpha/(\text{h cm}^2)$)	8-10 MeV Range ($\alpha/(\text{h cm}^2)$)
Day 3	69	$2.63^{+0.02}_{-0.02}$	$1.029^{+0.010}_{-0.010}$	$1.36^{+0.01}_{-0.01}$
Day 6	37.8	$0.031^{+0.002}_{-0.001}$	$0.012^{+0.002}_{-0.001}$	$0.013^{+0.002}_{-0.001}$
Day 11	72	$0.0083^{+0.0009}_{-0.0008}$	$0.0036^{+0.0006}_{-0.0005}$	$0.0011^{+0.0004}_{-0.0003}$
Day 16	132	$0.0066^{+0.0006}_{-0.0005}$	$0.0031^{+0.0004}_{-0.0004}$	$0.0007^{+0.0002}_{-0.0002}$

Table 5.1. Activity for copper exposed to four camping lantern mantles inside a stainless steel pressure cooker.

Days After Exposure	Run Duration (h)	Total Emissivity ($\alpha/(\text{h cm}^2)$)	5-7 MeV Range ($\alpha/(\text{h cm}^2)$)	8-10 MeV Range ($\alpha/(\text{h cm}^2)$)
Day 3	72	$0.061^{+0.002}_{-0.002}$	$0.022^{+0.001}_{-0.001}$	$0.023^{+0.002}_{-0.001}$
Day 6	24	$0.020^{+0.003}_{-0.002}$	$0.007^{+0.002}_{-0.001}$	$0.0011^{+0.0007}_{-0.0004}$
Day 7	24	$0.023^{+0.003}_{-0.002}$	$0.010^{+0.002}_{-0.002}$	$0.0003^{+0.0004}_{-0.0002}$
Day 8	24	$0.026^{+0.003}_{-0.003}$	$0.009^{+0.002}_{-0.002}$	$0.0016^{+0.0008}_{-0.0005}$

Table 5.2. Activity for copper exposed to four camping lantern mantles inside a glass jar.

We also monitored the decays over time and calculated the half-life for ^{212}Pb . Its daughter isotope ^{212}Bi decays by two primary methods and has a half life of 61

minutes. ^{212}Bi can decay into ^{208}Tl (thallium) via a 6.2 MeV alpha or ^{212}Bi can beta decay into ^{212}Po which then decays to stable ^{208}Pb via a 8.9 MeV alpha. ^{212}Po has a $0.3 \mu\text{s}$ half-life. Thus, the intermediate step happens immediately. Figure 5.6 illustrates the decays over time in the 5 to 7 MeV range corresponding to the ^{212}Bi peak. Figure 5.7 shows decays over time in the 8 to 10 MeV range corresponding to the polonium peak. The half-life is fitted to both exponential decays. Both obtained values are consistent with the 10.64 hour half-life for ^{212}Pb .

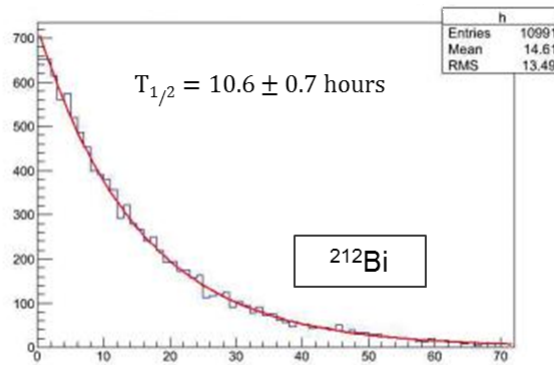


Figure 5.6. Bismuth decay via alpha in 5 to 7 MeV range

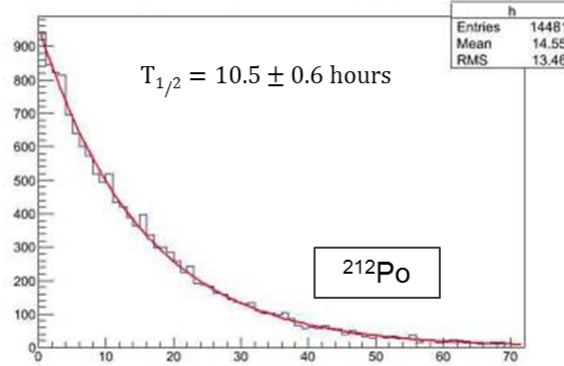


Figure 5.7. Polonium decay via alpha in 8 to 10 MeV range

At the 120th hour of measurement the activity for copper from the glass jar was $0.022 \pm 0.010 \alpha/(\text{h cm}^2)$. For the copper in the pressure cooker, this was also $0.022 \pm 0.010 \alpha/(\text{h cm}^2)$ within errors. Since the volume above the copper rectangle in the glass jar was three times the volume above the copper plate in the pressure cooker, we expected the emissivity from the glass jar's copper to be three times greater than the pressure cooker's copper. Instead we obtained the same emissivity. Scaling down the glass jar copper's activity by a third ($0.007 \pm 0.003 \alpha/(\text{h cm}^2)$) allowed us to directly compare the copper emissivities taking into account volume differences in the exposure vessel. The scaled emissivity is slightly low considering the error bars. One hypothesis to explain these results is that the activities of the camping mantles are not identical. Another possibility is that radon leaked out from the glass container since it was sealed with tape and aluminium foil, while the pressure cooker was airtight. In the future, the RAD7 machine can test the amount of radon in the glass container and pressure cooker to compare activity in the volume and test for leaking. Another possibility is that the charged daughter particles become attracted to the insulating walls. Exposing copper samples in an airtight glass vessel with the

same lantern mantles used in the pressure cooker will give us a more accurate test to compare radon plate-out onto a sample while housed in an insulating or conducting container.

REDUCTION OF RADON PLATE-OUT ON COPPER UNDER NITROGEN PURGE

A common method to mitigate radon exposure used in labs around the world is to store detector components under boil-off nitrogen purge inside of gloveboxes and purge cabinets. Boil-off gas from a dewar of liquid nitrogen is used to guarantee high purity nitrogen with a low level of contaminants. The idea is to prevent radon levels from accumulating by constantly pushing out nitrogen from the chamber. This study will compare the effectiveness of using nitrogen purge by comparing the activity on copper plates that have been exposed to a thorium source under different flow rates. The eventual goal for this study is to find an optimal flow rate that effectively prevents radon progeny from sticking to the copper. The flow rate must also be low enough to conserve liquid nitrogen to avoid raising the cost for low radioactivity physics experiments.

6.1. Experimental Setup

Three copper plates were placed on a 3D printed plastic holder or a stainless steel holder as illustrated in Fig. 6.1. The top side of the copper plates were labeled "Cu1", "Cu2", and "Cu3" with the experiment name for identification. Cu1 was placed on the bottom shelf of the holder. Cu2 was placed on the third rack from the top while Cu3 was placed on the top rack. This experimental set up is illustrated in Fig 6.2. A modified stainless steel pressure cooker with added ports housed the holder and served as the exposure chamber. At the bottom of the pressure cooker, there were

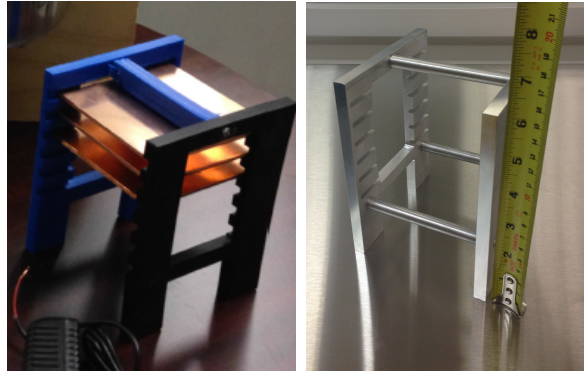


Figure 6.1. Left: 3D printed plastic holder used for purgeless control experiment. Right: Stainless steel holder of similar dimensions

eight 1900s camping lantern mantles which contain ^{232}Th . Boil off nitrogen entered through tubing attached to the pressure cooker lid and exited through a flow meter at the bottom of the pressure cooker. Since the volume was constant, the flowrate was set and monitored at the outflow. Between each experiment, the pressure cooker and copper holder was cleaned with a RadiacWash towelette, rinsed with deionized water, and rinsed with isopropyl alcohol.

The standard flowrate in the LUMINA purge box is 4 standard cubic feet per hour (SCFH) which is equivalent to 104 NCMH or normal cubic meters per hour. The pressure cooker height was 0.61 feet while the radius was 0.34 feet. This makes the volume of the exposure vessel 0.22 cubic feet. We divided the volume by the flowrate to calculate how long it takes to replace the nitrogen inside the exposure chamber. This study used two purge rates 3 SCFH and 6 SCFH with copper placed on the stainless steel holder. With the 3 SCFH flow rate, the vessel refilled with new nitrogen every 5 minutes. With the 6 SCFH flowrate, the purge replaced the vessel volume every 2 minutes. We compared this to the 55.6 second half-life of ^{220}Rn . A



Figure 6.2. Purge Experiment Set Up

purge rate of 6 SCFH allowed for 2.4 half-lives of ^{220}Rn before pushing all the nitrogen out while the 3 SCFH purge rate allowed for 5 half-lives. Both purge rates replaced the volume much faster than the 3.82 day half-life of ^{222}Rn which is not used in this study. If we had used ^{222}Rn , a lower purge rate would probably be sufficient. A control experiment was run using the plastic holder placed in an airtight nitrogen backfilled pressure cooker with no air flow for comparison. Each vessel was exposed to the same eight lantern mantles placed using the same position map for five days. Immediately after opening the pressure cooker, the samples were placed in the XIA UltraLo-1800 to count them.

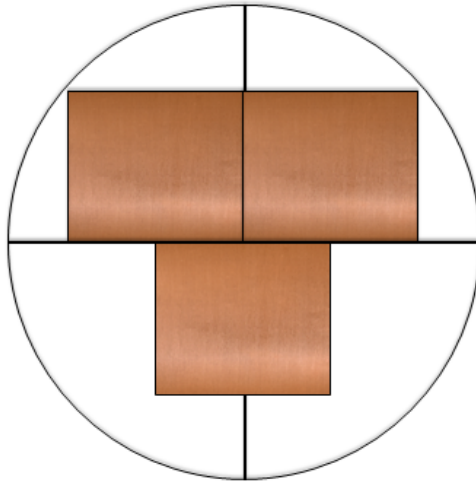


Figure 6.3. When counting in the XIA machine, the copper is placed forming a T-shape with Cu1 at the top left, Cu2 at the top right, and Cu3 at the bottom

Only the bottom side of each copper plate is counted. The copper plates are placed in the 707 cm^2 wafer sized counting region forming a T shape with the edges touching as illustrated in Fig 6.3.

6.2. Results

Figure 6.4 illustrates data points for the copper from the control experiment, 3 SCFH purge rate, and 6 SCFH purge rate.

We fit the data using equation 1.5. Since the 61 minute half-life of ^{212}Bi is much longer than the $0.3 \mu\text{s}$ half-life of ^{212}Po , the secular equilibrium case applies and we can assume the activity rate of bismuth stays roughly constant in comparison to polonium.

Experiment	Emissivity($\alpha/(\text{h cm}^2)$)
Pure Control	26.8 ± 0.3
3 SCFH Purge	0.42 ± 0.04
6 SCFH Purge	0.31 ± 0.03

Table 6.1. Emissivities at the 40th hour of measurement for purge Experiments

To compare the runs, we decided to compare the emissivities of the three copper samples at the 40th hour of measurement. These values are reported in Table 6.1. The 3 SCFH flowrate is effective in removing 98 ± 7 % of the radon contamination compared to the control. The 6 SCFH flowrate is effective in removing 97 ± 6 % of the contamination. Oddly, the 6 SCFH flowrate resulted in a higher copper plate activity than the 3 SCFH flowrate. We have two hypothesis to explain this result. There are some differences between the 6 SCFH experiment and the 3 SCFH experiment other than the flow rate. We discovered a leak from the top bolt when running the 6 SCFH experiment about 5 hours after the start of exposure and found the initial purge rate was greater than intended. This is unlikely to have caused the discrepancy. We also noticed that the 6 SCFH vessel was over pressurized when we opened it while the 3 SCFH vessel was not over-pressurized. It is possible the over-pressurization resulted in the discrepancy. Additional testing is required to validate these hypothesis.

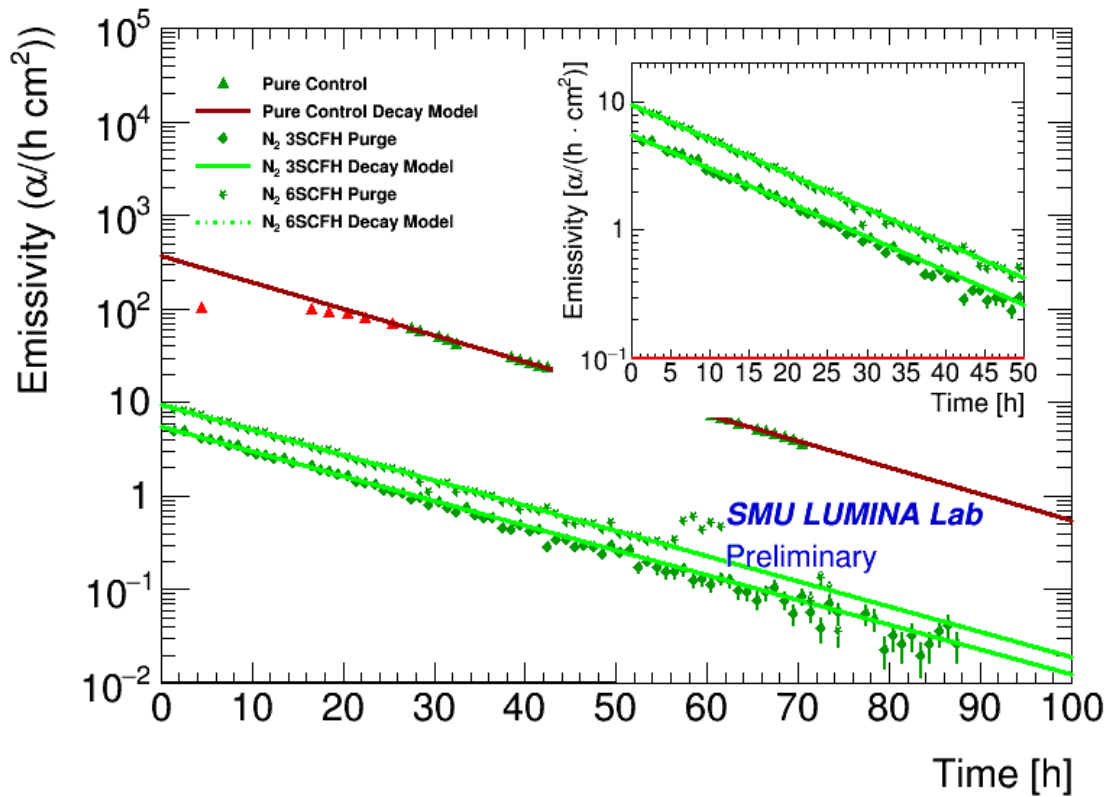


Figure 6.4. Here are the results from the control and two purge rate experiments. The red line represents the double radioactive species exponential fit to data from the control experiment in a closed vessel without purge. The red triangles represent rejected data points with activities above the measurement limit of the XIA machine. The solid green line with diamond shaped data points represents the copper from a 3 SCFH purge while the green line with star shaped data points represents the copper from a 6 SCFH purge.

Chapter 7

Study of Radon History in SuperCDMS at Soudan

The previous chapters dealt with radon plate-out studies onto various materials using the XIA UltraLo 1800 alpha particle counter. In this chapter, I describe work using data for radon levels in the air in various labs that house SuperSCMDS Soudan detectors to estimate the background activity rate from ^{222}Rn for these detectors. The history of each detector is kept in a log book. This includes the location of the detector and activities such as fabrication, shipping, polishing, housing, etc. All entries in the log specify when the detector was received and shipped off as well as the duration of some procedures performed on each detector. The time spent in each lab is added up for dates between June 2011 and early October 2011 for the detectors G41, G42, G43, G24S, G53, G2E, G48, G47, G52, G21P, G50, G20O, G51, G19N, and G7F. The locations in the study are Tunnel C, Center for Integrated Systems (CIS), Radon Suppression Facility (RSF) at Stanford University, CORE, University of California Berkeley (UCB), University of Minnesota (UMN), He3, and SLAC National Accelerator Laboratory in addition to a shipping vessel and a purge bag.

The radon measurements used for each location are in the Table 7.1. We assumed the purge boxes and polycarts in all locations had the same concentration of radon as the CIS under purge. Average ambient rates for the CIS, RSF, and SLAC were provided by Ms. Astrid Tomada. The radon exposure rate for various locations were drawn from background measurements taken at facilities used by the CDMS collaboration.

Location	Radon (Bq/m^3)
Tunnel C	76
Tunnel C under Purge	0.61
CIS	10.6
CIS under Purge	0.56
RSF	4.28
RSF in Polycart	0.56
CORE	9
UCB assembly time	85
UCB in Polycart	0.56
UMN Cleanroom	8.6
UMN Little Blue Clean Tent	8.6
UMN Vaccume or Clean Gas	0.56
UMN in Purge Cabinent	0.56
UMN Clean Bench	8
SLAC in Polycart	0.56
SLAC	10.7
He3	0
Shipping Vessel	0.1
Purge Bag	6

Table 7.1. Radon backgrounds at SuperCDMS Facilities

We assumed the detectors were encased in either copper, plastic, or protected by photo-resist unless being worked on while in CIS or RSF. While the detectors were in CIS, we assumed the open detector face was worked on and exposed for a third of the time and under purge for the remaining time. The assumed plate-out rate, p , is 1%. This plate-out rate is the efficiency for a daughter of radon to stick to a surface. We do not have measurements for plate-out onto germanium at this time but 1% is the plate-out rate onto nylon in a cleanroom [7]. The column height, h , is assumed to be 0.5 ± 0.3 m in the open air and 0.05 ± 0.03 in copper or plastic housing. We estimate the activity rate, A , in events/(day cm^2) each detector using:

$$A = 8.64\lambda phrt \tag{7.1}$$

Here, r is the radon level in the Table 7.1 and t is time. The 8.64 factor is used to convert from meters to centimeters and day to seconds. λ is the decay constant for ^{210}Pb which is $8.55 \times 10^{-5} \text{ s}^{-1}$. The resulting activity for each detector illustrated in Fig. 7.1:

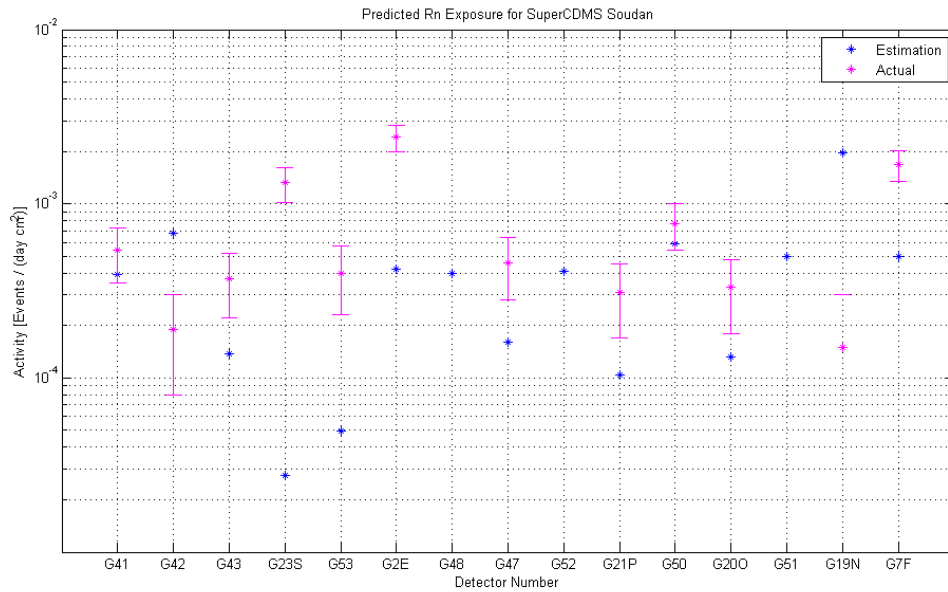


Figure 7.1. Estimated background activity for SuperCDMS in Soudan. The detectors are ordered sequentially from T1Z1 to T5Z3.

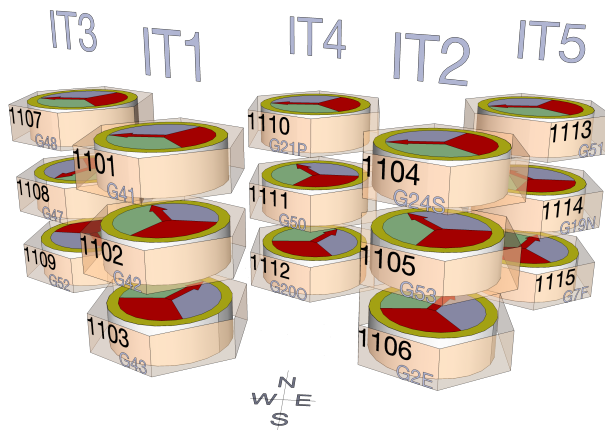


Figure 7.2. Tower arrangements for SCMS Soudan

Figure 7.2 illustrates the detector arrangements. This gives us a relative comparison between the different detectors and provides us a baseline for expected activity. We evaluated our predictions by comparing estimated emissivities to measured emissivities [3]. Detectors G48 and G52 purposely have a lead plate next to them so their measured activity is high and is not compared to our estimation. A couple of the estimations fall within the error bars of the measured activity. The alpha rates measured from the detectors average at $(7.5 \pm 0.8) \times 10^{-4}$ events/(day cm^2). The average activity in our estimation is $(4.3 \pm 0.4) \times 10^{-4}$ events/(day cm^2). Estimation errors can be due to various reasons such as incorrect assumptions about the column height at each location. Column height may be more complicated than this estimation assumes. In addition, radon levels vary seasonally. Also, the log book entries for detector histories vary depending on the institution housing the detector. Some institutions include more details than others.

Chapter 8

Conclusion

Over the past four years, we have completed numerous studies involving backgrounds due to ^{222}Rn in dark matter experiments. We have studied the charge collection efficiency at various positions of the XIA UltraLo-1800 using a one-inch diameter calibrated ^{230}Th source. We find the measurement efficiency is symmetric about the polar angle and is highest at the center of the tray. Collection efficiency decreases further from the center of the tray. This study shows promising results for developing our own efficiency correction for sources smaller than the 707 or 1800 cm^2 tray configuration.

We have evaluated cleaning procedures for acrylic for the MiniCLEAN direct dark matter search. Removing the top millimeter of material is effective in removing 96 % of the contamination from ^{210}Pb and ^{210}Po in the region of interest between 4 - 6 MeV. Plasma etching by the IntIVac company removes 20% more contamination than the control in the region of interest. The control was not cleaned but 41.9 % of the contamination is removed simply by shipping and handling the sample. This suggests that majority of the ^{222}Rn daughters are on the surface of the material and do not penetrate deep into the acrylic.

We have conducted a preliminary study to determine whether storage inside a conductor or an insulator effects ^{220}Rn plate-out by exposing copper plates inside a glass jar and stainless steel pressure cooker. We outlined future studies on the leaking of ^{220}Rn through the tape seal on the glass jar in order to interpret the results of our study. The future study will use a RAD7 machine which counts the amount of ^{222}Rn

or ^{220}Rn in the air to monitor activity levels inside the glass jar and pressure cooker.

We have also conducted preliminary studies to find an optimal boil-off nitrogen purge rate to keep ^{220}Rn away from copper samples. The copper from an over-pressurized 6 SCFH purged vessel had a higher activity than copper from a 3 SCFH purged vessel that was not pressurized. A confirmation experiment is needed to confirm results. These studies are helpful to inform design decisions in future dark matter searches. In addition, we estimated the activity rate due to ^{222}Rn contamination of the SuperCDMS Soudan detectors based off of exposure history in various labs across the United States.

Over the years, we learned how to operate the XIA UltraLo-1800 and minimize background activity by covering the empty tray and developed software to analyze results. We were among the first five institutions to use this instrument to characterize radioactive background rates of various materials. We used the alpha particle counter to study radon plate out in a variety of environments and evaluate cleaning procedures to mitigate radon contamination. These studies may help inform the design of future dark matter experiments.

Appendix A

Radon Monitoring in LUMINA Lab

Radon levels in our lab have been monitored with a RAD7 machine over the past few years. With help of Read Oak High School teacher Janee Hall, we have exported and collected the data and plotted radon levels over time. We then decoded Automated Surface Observing System (ASOS) data from Dallas Love Field Airport to investigate seasonal variations in radon levels in our lab. The seasonal weather factors are plotted along side laboratory radon measurements in Fig A.1. Lower pressures usually correspond to higher radon levels except during the summer and autumn of 2012 during which we had unusually low amounts of radon for the summertime. Areas of lower air pressure also tend to be days where the air pressure fluctuates more than other times of year. Rises in radon levels also seem to correspond to dips in relative humidity. Indoor and outdoor temperatures follow the same trend as each other and have an inverse relationship with air pressure and follows an inverse correlation with radon levels. On average, radon levels tend to increase during the summer and decrease during the winter. The radon levels also fluctuate depending on how often the doors are opened and the building is in use.

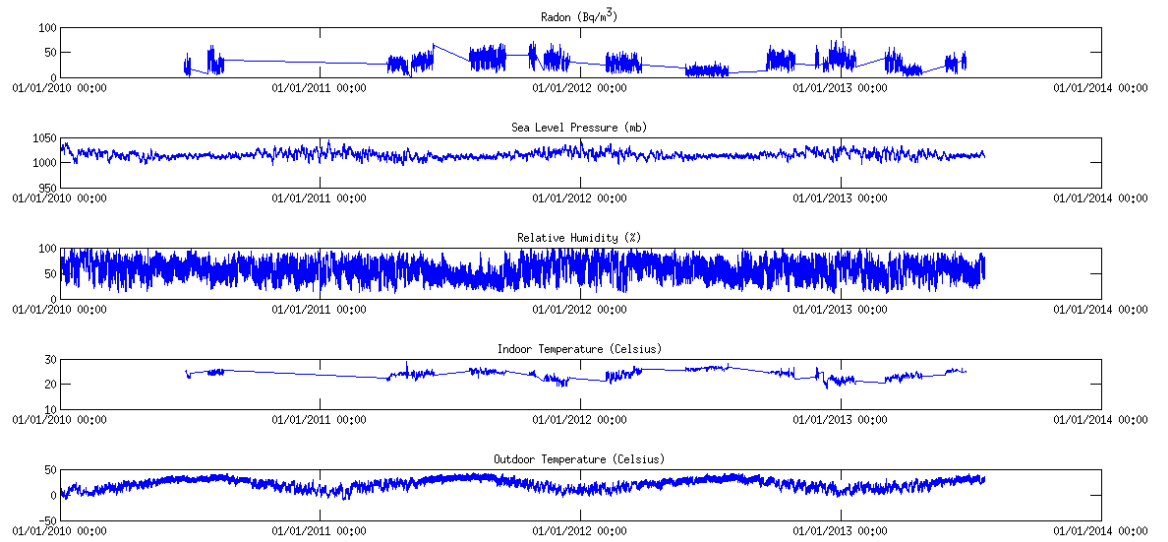


Figure A.1. Radon levels in the LUMINA lab over time compared to weather. In this plot, humidity is not corrected for when calculating radon levels off of a RAD7 machine

Appendix B

Appendix: XIA Efficiency Correction

When an alpha particle's track crosses the border of the counting region, it cannot be distinguished from an emission from the side walls of the XIA counter [4]. The event gets rejected and classified as a sidewall event rather than an alpha particle. XIA provides an efficiency correction to account for this effect based on a combination of analytical computations using a calibrated check source and Monte Carlo simulations. These corrections are most accurate for a large number of alphas and assumes the sample covers the entire counting region. When calculating emissivities, alpha events are summed into 10 energy bins and divided by these numbers provided by XIA.

Bellow is the efficiency correction table from the XIA User's Manual:

E_{α} (MeV)		Efficiency Corrections $\langle \Omega_{\epsilon} \rangle$	
Energy Range	$\langle \text{Avg} \rangle$	Full Config.	Wafer Config.
$0 \leq E < 1$	0.5	1.0000	1.0000
$1 \leq E < 2$	1.5	0.9816	0.9740
$2 \leq E < 3$	2.5	0.9672	0.9542
$3 \leq E < 4$	3.5	0.9497	0.9306
$4 \leq E < 5$	4.5	0.9290	0.9035
$5 \leq E < 6$	5.5	0.9052	0.8736
$6 \leq E < 7$	6.5	0.8790	0.8424
$7 \leq E < 8$	7.5	0.8505	0.8102
$8 \leq E < 9$	8.5	0.8188	0.7769
$9 \leq E < 10$	9.5	0.7876	0.7467

UltraLo-1800 Efficiency correction provided by XIA in the User's Manual

REFERENCES

- [1] *Ultra-low Background Alpha Particle Counter Using Pulse Shape Analysis* (October 2004), vol. 1, IEEE Nuclear Sci. Symp Conf. Rec.
- [2] B. D. McNALLY; W. K. Warburton; S. Coleman, J. A. B. M. C. J. C. M. S. G. Z. Z. Multicenter comparison of alpha emissivity measurements using the ultralo-1800 alpha particle counter. Tech. rep., XIA LLC, 2012.
- [3] CALKINS, R. "http://titus.stanford.edu/cdms_restricted/Soudan/R133/ebook/131028_rc_update/V4/tables.html, Oct. 2013.
- [4] LLC, X. *UltraLo-1800 Alpha Particle Counter User's Manual*. XIA LLC, 2013.
- [5] MOOK, W. G. *Environmental Isotopes in the Hydrological Cycle*, vol. 1. International Atomic Energy Agency and United Nations Educational, Scientific, and Cultural Organization, 2000.
- [6] R. AGNESE, E. A. Demonstration of surface electron rejection with interleaved germanium detectors for dark matter searches. Tech. rep., 2013.
- [7] SHUTT, T. Personal communication.
- [8] W. K. Warburton, J. W., AND MOMAYEZI, M. Ultra-low background gas-lled alpha counter, 05 2014.